# Proof-of-Concept of GNSS-based Phase Synchronization for Bistatic and Multistatic SAR Missions.

Eduardo Rodrigues-Silva[a], Marc Rodriguez-Cassola[a], Alberto Moreira[a], Gerhard Krieger[a], and Steffen Thölert[b]

[a]Microwaves and Radar Institute, German Aerospace Centre (DLR), Oberpfaffenhofen, Germany
[b]Institute of Communications and Navigation, German Aerospace Centre (DLR), Oberpfaffenhofen, Germany

## Abstract

This paper addresses the critical issue of phase synchronization in multistatic SAR. We present the experimental validation of a GNSS-based method planned for use in the upcoming ESA's Earth Explorer Harmony mission, where both the radar payload and GNSS receiver utilize the same oscillator. The paper outlines the experimental procedure for assessing the achievable accuracy and calibrating covariances. It presents a point-to-point estimation and a smoothing approach based on a stochastic description of phase noise. The technique achieved in a lab environment relative synchronization errors below 515 fs (1 $\sigma$), or 1 degree for a 5.4 GHz radar system.

## 1    Introduction

Following the trend towards small satellites, many bistatic and multistatic spaceborne SAR concepts have been proposed recently, such as the mission concepts described in [4, 8]. All of those bistatic and multistatic concepts depend on accurate synchronization of the radar payloads, which, in general, presents one of the most critical challenges in bistatic and multistatic SAR systems. In addition, the potential benefits that add-on missions like the planned ESA's Earth Explorer Harmony mission may offer in the future underscore the need for standardization in synchronization solutions.

Very few bistatic systems have been successfully demonstrated in space. The pioneer in demonstrating bistatic operations on separate platforms was TanDEM-X [6], achieving unparalleled DEM accuracy. More recently, the LuTan-1 bistatic mission successfully demonstrated the operation of a bistatic SAR system in L-Band. Both missions relied on synchronization links [9, 7], which could be too costly, complicated, or even unfeasible on system concepts using three or more satellites.

GNSS systems have been used for synchronization of different kinds of systems for decades [10]. In [11], the author gives an overview of GNSS-based synchronization techniques and evaluates the synchronization of a ground-based tri-static pulsed-doppler networked radar system using GPS-disciplined oscillators. Good performance for the proposed application was reported, but it is insufficient for SAR imaging and interferometric applications. In [12], the author proposes using the GNSS technique for space applications, in which PPS signals from the GNSS receiver are used to discipline the radar oscillator of the transmitting and receiving systems, considerably reducing the differential phase drifts, but still mainly relying on data-based approaches to correcting the remaining residuals.

We proposed in [2] a GNSS-based synchronization tech-

nique based on the common-view carrier phase measurements in which the radar payload and the GNSS receiver share the same master oscillator. This synchronization concept requires only an accurate, precise baseline determination, which is already required for most use cases of bistatic and multistatic systems. The technique is trivial to implement in hardware, and it does not require any signal exchange between the satellites, making it an ideal synchronization solution in terms of simplicity, scalability, and ease of integration between different systems. The concept was selected as the nominal synchronization for the Harmony mission.

The work described in this paper assessed the technique and investigated in which conditions it works with commercial receivers. The following sections demonstrate that the technique can achieve high synchronization accuracy with current GNSS technology in a lab environment.

The paper is organized as follows: In the next section, we explain the GNSS-based synchronization technique in general terms. In the third section, we explain the experimental methods to calibrate the estimation algorithm and assess the achievable accuracy of the technique with a given GNSS receiver. In the fourth section, we show the experimental results, and in the last section, we summarize the conclusions of the experiments.

## 2    GNSS-based phase synchronization

Figure 1 illustrates the fundamental hardware architecture required for GNSS-based synchronization. In this proposed design, a single Ultra Stable Oscillator (USO) generates the radar and reference signals within the GNSS receiver. While the figure depicts a transmitter and receiver, it is important to note that this concept is equally applicable to multiple receive-only systems. Within the GNSS re-
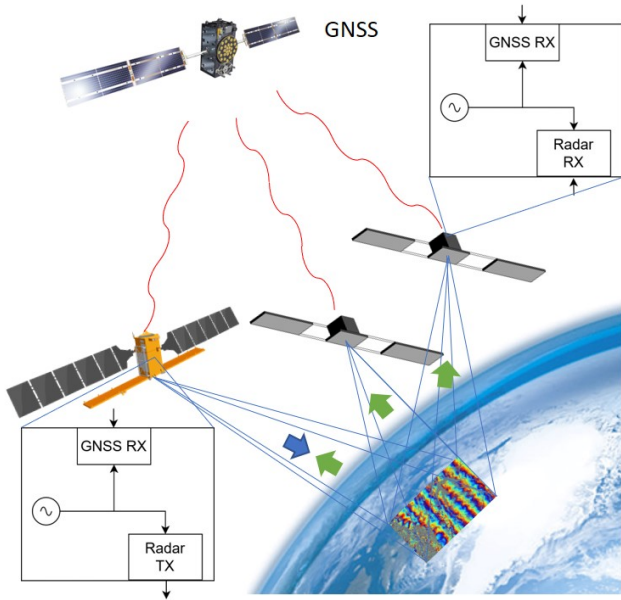
**Figure 1** GNSS-based phase synchronization scheme (Satellite models credits: ESA).

ceiver, the GNSS signal undergoes down-conversion, and then it is compared to an internally generated GNSS code and carrier at an intermediate frequency. The receiver generates the signal for downconversion and the reference GNSS signal coherently from the master oscillator. In this configuration, the carrier phase measurement (in units of meters) contains information about the range variation between the GNSS receiver and transmitter and differences in clock drifts, as expressed in the Equation (1).

$$L_{uv,k}^{(i)}(t) = \rho_{uv}^{(i)}(t) + c \cdot \delta t_{uv}(t) - \left(\frac{\lambda_k}{\lambda_1}\right)^2 \cdot I_{uv}^{(i)}(t) -$$
$$\lambda_k \cdot A_{uv,k}^{(i)} + M_{uv,k}^{(i)}(t) + \epsilon_{uv,k}^{(i)}(t), \qquad (1)$$

where $\rho_{uv}^{(i)}$ is the difference between the distances from receivers $v$ and $u$ to the $i$-th navigation satellite, respectively, c is the speed of light in vacuum, $I_{uv}^{(i)}$ is the difference between the biases caused by the ionospheric delays for a signal at wavelength $\lambda_1$, $A_{u,k}^{(i)}$ is the ambiguity, $M_{uv,k}^{(i)}(t)$ describes other systematic error components including multipath, cross-talk, tracking channel bias and phase wind-up, and $\epsilon_{uv}^{(i)}(t)$ is residual error component, including thermal noise.

The following biased estimate of the phase difference between the oscillators' signals over time can be derived from this measurement model [2]:

$$\tilde{\psi}_{uv,0} = \frac{2\pi}{\lambda_0} \cdot \sum_{i=1}^{N} \sum_{k=1}^{n_\lambda^{(i)}} \alpha_i \cdot \frac{L_{uv,k}^{(i)} - \tilde{\rho}_{uv}^{(i)}}{n_\lambda^{(i)}}, \qquad (2)$$

where $\alpha_i$ are weighting factors dependent on the signal-to-noise ratio of the signal, $N$ is the number of GNSS satellites, and $n_\lambda^{(i)}$ is the number of signals transmitted by GNSS satellite $i$. This equation assumes that the satellites are close enough so the differential ionospheric delay is negligible (< 1 km). Only GNSS data acquired continuously during the whole acquisition period are used. Each scaled motion-compensated carrier phase (see the term in the summation in (2)) is an estimate of the phase difference between the oscillators. These estimates are weighted according to the estimated thermal noise and the measured correlation between the clock contamination term between signals.

In conventional navigation applications, the internal clock in a GNSS receiver is, by default, filtered and steered to match the GPS time, minimizing the clock offset estimated in the navigation solution. This means the coherence between the internal receiver reference and the external oscillator is usually lost by default. The receiver tracking performance is specified in terms of the thermal noise, which does not include any clock tracking error. In summary, a high coherence between internal and external frequency references is usually unnecessary. Therefore, we cannot expect conventional receivers to be designed to fulfill the level of accuracy necessary for SAR synchronization. Needless to say, the aforementioned clock steering has to be disabled in case the receiver is used for synchronization in the way described in this paper.

The coherence between the external reference and the internal reference GNSS signals can be determined by calculating the single differences of the carrier phase measurements between two receivers taking as input the same GNSS signal (e.g., using the same antenna) and the same master oscillator, as illustrated in Figure 2. Results from such experiments are reported in [5], where the authors show a higher standard deviation from the carrier phase single differences than expected from the specifications. This indicates a contamination of the reference phase within the receiver.

The experimental evidence in the literature points to a phase error introduced within the GNSS receivers, which might dominate the phase error budget for bistatic SAR and still have little impact in most conventional GNSS applications. In light of these results, we conclude that a better understanding of the reference tracking capability of GNSS receivers is necessary for assessing the technique's full potential.

The first objective of the concept validation experiments detailed in this paper is to verify if the synchronization scheme can be readily implemented with current technology in a relevant laboratory environment. The second objective of this paper is to propose a method of determining the optimal weighting factors $\alpha_i$ of each carrier phase measurement based on experimental characterization of the GNSS receivers and, finally, to suggest a filtering approach for the data.

## 3 Experimental method and calibration

### 3.1 Hardware setups and results assessment

The figures 2, 3 and 4 below illustrate the experimental setups used. For all the experiments using an indepen-

dent oscillator to drive each receiver, the phase between the oscillators is measured simultaneously using an independent device. The device is configured for a bandwidth of 100 Hz. In each experiment, the independent relative phase data acquisition begins before the acquisition with GNSS and ends after the acquisition with GNSS. The reference is undersampled to match the sampling rate of the GNSS data and correlated until the peak is found to allow for the alignment of the two independent sets of measurements. The undersampling is done for all the possible data combinations, and the data set of maximum correlation is selected. Finally, the data obtained through GNSS and the independent instrument are compared, and the estimation errors are assessed.

For the short baseline experiments, the differential range histories from GNSS satellites to the fixed antennas are used to calibrate the carrier phase measurements, as indicated in Equation 2. The data assessment is illustrated in Figure 5.
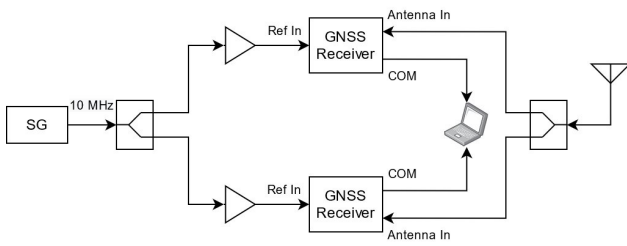


**Figure 2** Common oscillator, zero baseline experimental setup.
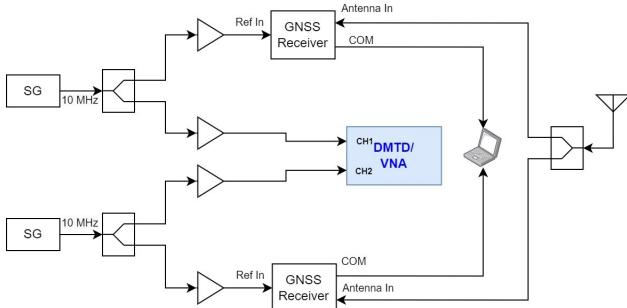


**Figure 3** Two oscillators, zero baseline experiment setup.
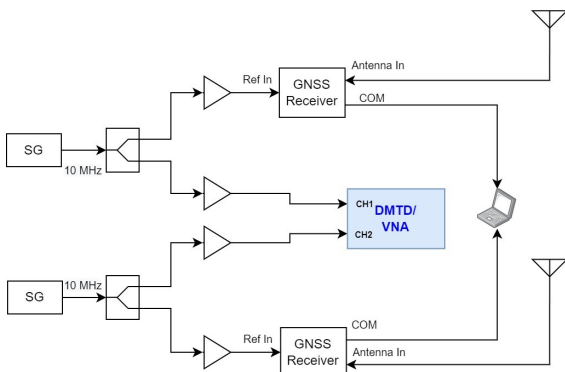


**Figure 4** Two oscillators, short baseline experiment setup.
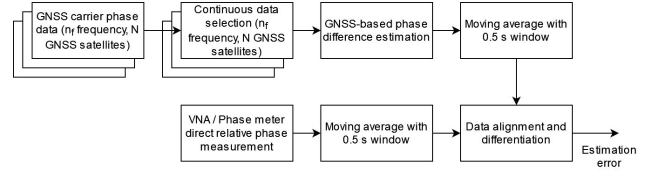


**Figure 5** Data processing and comparison to reference.

A moving average filter is applied to the reference to emulate the effect of the SAR processing on the phase noise component of the data.

Two different receivers were used: the OEM729 manufactured by Novatel, which is a product aimed at mass production for a broad range of applications, and the PolaRx5TR receiver manufactured by Septentrio, a more specialized equipment targeted at high-performance time-transfer and geodetic applications.

## 3.2 Covariances matrices measurement

The receiver-induced error calibration procedure is done from the setup illustrated in Figure 2. In this setup, most of the terms in the differential carrier phase, expressed in Equation (1), cancel out. In an ideal case, the differential carrier phase obtained in this experiment would consist of a constant signal plus a noise component in line with the thermal noise specification of the receiver. However, we observed that the noise level of the differential carrier phase experiment is above the specifications, and additionally, the errors are correlated for different carrier phase measurements. This correlation depends mostly on the type of signal being tracked but is fairly independent of the GNSS satellites from which it originates. In particular, the GNSS signals belonging to the newest third frequency band E6 for Galileo and B3 for BeiDou presented a much lower correlation with other signals for the PolaRx5TR time-transfer receiver tested, as shown in Figure 6.

These observations motivated the development of the calibration technique of the covariance matrix of the phase-tracking errors in the differential carrier phase measurements. This calibration technique is presented below.

The main assumption is that while the diagonal terms of the covariance matrix of the carrier phase measurements depend on several circumstantial factors, such as elevation and multipath level, the off-diagonal terms are systematic and depend only on the signal types. Calculating the correlation between the phase tracking error of the carrier phase signals allows us to weight the differential clock estimation appropriately, which can result in a significant accuracy increase.

Assuming carrier phase measurements $L_{uv,k}^{(i)}$ are available from a common oscillator, zero baseline experiment, the off-diagonal terms of the matrix can be estimated as follows:

$$\hat{R}_{k,l} = \frac{4\pi^2}{\lambda_0^2 \cdot N \cdot (N-1)} \cdot \sum_{i=1}^{N_{kl}} \sum_{j=i+1}^{N_{kl}} \text{Cov}\left(L_{uv,k}^{(i)}, L_{uv,l}^{(j)}\right)$$

$$(3)$$
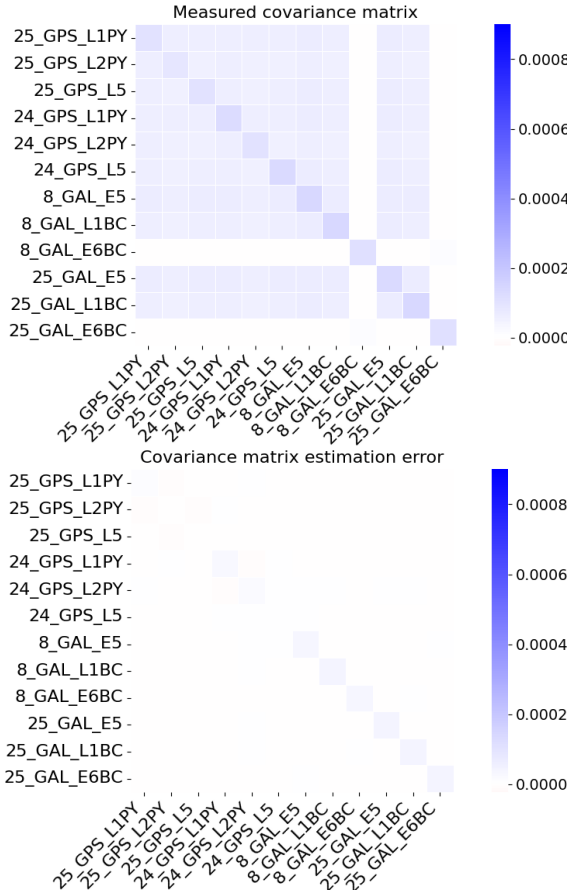
**Figure 6** Samples of covariance estimation results for the single oscillator, zero baseline experiment with the PolaRx5TR receiver.

The diagonal matrix can be estimated from the motion-compensated double-differences as follows:

$$
\hat{R}_{k,k}^{(i)} = \frac{4\pi^2}{\lambda_0^2 \cdot (n^{(i)} - 1)} \cdot \sum_{\substack{i=1 \\ i \neq j}}^{n^{(i)}} \mathrm{Cov}\left(L_{uv,k}^{(i)} - \tilde{\rho}_{uv}^{(i)}, L_{uv,l}^{(j)} - \tilde{\rho}_{uv}^{(j)}\right)
$$
$$
+ \hat{R}_{k,k}
$$
$$(4)$$

The effectiveness of the estimation can be assessed in a two-oscillator, zero-baseline experiment. Figure 6 below shows the estimated vs measured covariance matrix and the resulting error.

The main conclusion from the calibration procedure done for the two different receivers is that the precautions for maintaining the spectral purity of the oscillators associated with time-transfer receivers significantly decrease the correlation between the error in the carrier phase measurements.

### 3.3 Remarks on filtering approaches

Given the short duration of the SAR data acquisition and the proximity of the noise in question to the carrier, the 1/f term of the phase noise signature will be predominant in the measurements, and the phase noise can be well mod-



**Figure 7** Antenna placement in the experiments with the PolaRx5TR receivers.

eled as a random walk, which corresponds to the integration of a gaussian noise process. Based on this assumption, a Kalman filter can be designed from the trivial model below:

$$
x_{uv,0}[k+1] = x_{uv,0}[k] + n \,, \tag{5}
$$

where $x_{uv,0}$ is the point-by-point detrended phase estimate at the radar carrier, and $n$ is a Gaussian process noise, whose covariance term can be derived from the stability specifications of the oscillator in the time domain, or calculated from direct phase difference measurements between oscillators of same model in a controlled environment.

Alternatively, or additionally to the Kalman filter, empirically tuned least square smoothing could be used. Either way, the power of error components - mainly oscillator tracking error and multipath - limits the effectiveness of a filtering approach in the same bandwidth as the legitimate phase noise signatures originating from the oscillators. Therefore, the more concentrated the oscillator power is around the main frequency, the more errors we can eliminate through filtering. In this sense, the high short-term stability required for radar payloads will favor the error budget of the GNSS-based technique presented here. In the end, the error budget for a specific system will depend mainly on the phase noise signatures of the oscillators, how successful the multipath isolation and/or suppression is, and the phase-noise characteristics of the master oscillator.

## 4 Experimental results

The antenna placement in the experiment with the PolaRx5TR is shown in figure 7. Due to the proximity to buildings and trees, we can assume this to be an environment with high multipath.

The main experimental results from the two oscillators, zero baseline experiments, are shown in Figure 10.

The results are excellent for the PolaRx5TR time transfer receiver, almost comparable to what can be obtained with a synchronization link. The results were considerably worse for the OEM729, although still acceptable for
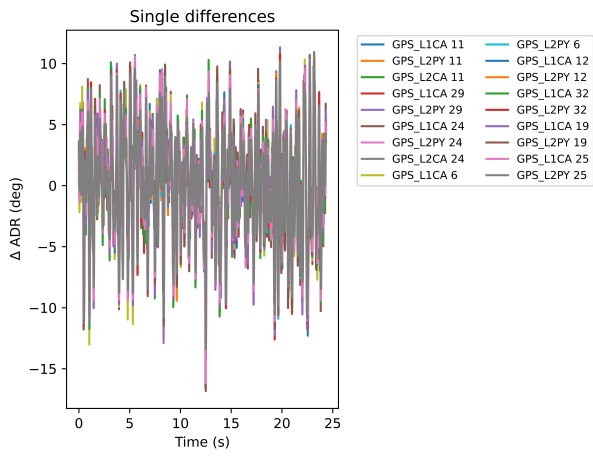
**Figure 8** Carrier phase single differences for single oscillator, zero baseline experiment with the OEM729 receiver.
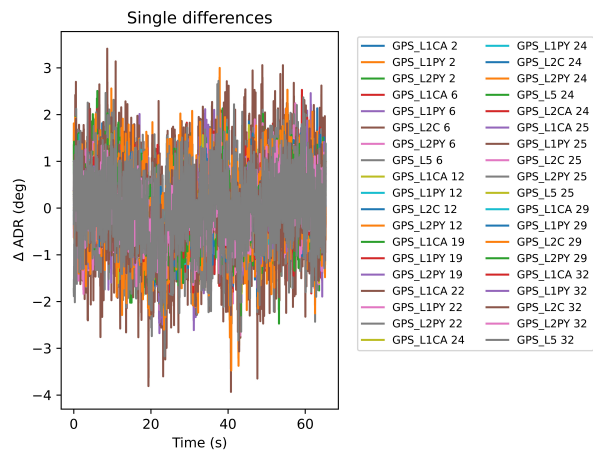


**Figure 9** Carrier phase single differences for the single oscillator, zero baseline experiment with the PolaRx5TR receiver.
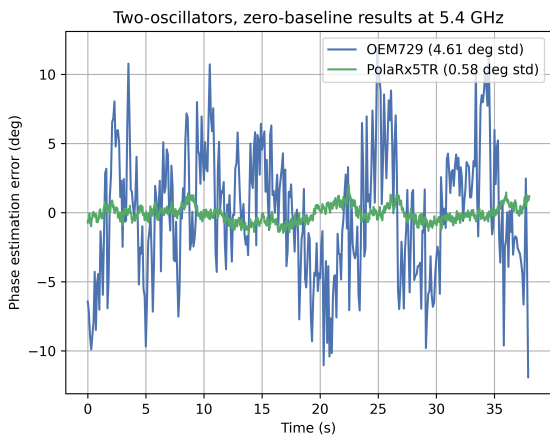


**Figure 10** Synchronization results for two oscillators, zero baseline experiment with the PolaRx5TR receiver.

lower frequencies, such as L-band, and less stringent SAR products. The difference is most likely due to possible precautions with the maintenance of the spectral purity of
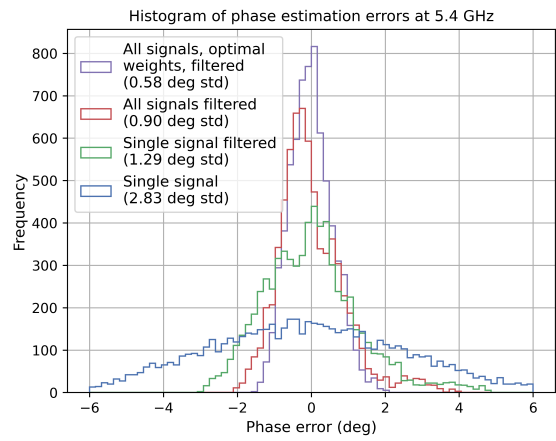


**Figure 11** Phase synchronization error histograms for different processing steps for a zero-baseline, two oscillators experiment with PolaRx5TR receivers.
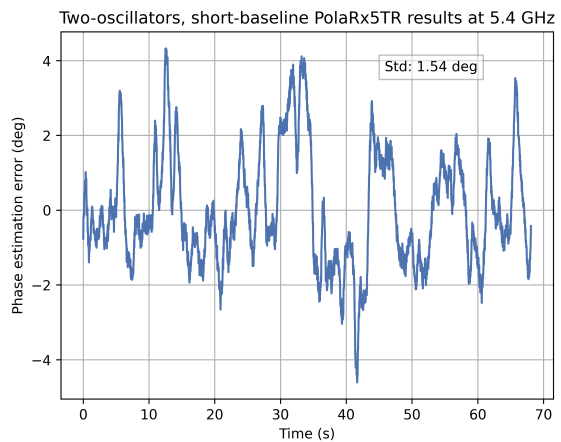


**Figure 12** Synchronization results for two oscillators, short baseline experiment with the PolaRx5TR receiver.

the master oscillator associated with state-of-the-art time-transfer GNSS receivers. The high covariances between all the different tracked signals in the OEM729 revealed this contamination of the clock path, leading to limited performance. The difference in clock contamination can be observed by comparing the differential clock tracking error on the carrier phases, shown in Figures 8 and 9. We can see a high correlation on the OEM729 differential carrier phase measurements, while for the PolaRx5TRs, the errors seem fairly uncorrelated.

Figure 11 shows the synchronization results using the PolaRx5TRs for different processing steps applied. We can see that proper filtering and weighting based on characterizing the carrier phase measurements and oscillator phase noise largely improves the synchronization results.

Figure 12 shows the results from the two oscillators, short-baseline experiment. This experiment is the first assessment of the technique at the system level. Excluding the independent phase measurement setup, which would not be present in the real application, the two sets of reference oscillator, receiver, and antenna are completely physically disconnected and could be embedded at separate platforms.

The results reveal a pronounced increase in phase error, albeit acceptable, particularly for L-band systems. It is worth noting, however, that in a spaceborne application, multipath interference is expected to be significantly lower, making the results depicted in Figure 10 more indicative of an operational scenario. Another contributing factor to the performance discrepancy in this context is that one of the experiment's antennas had limitations in tracking the newest third-band signals, which were shown to have a low correlation compared to the others for the PolaRx5TR receivers.

An important conclusion drawn from this study is that performance can be improved through precautions in receiver design to prevent clock path contamination and potentially through adjustments in the configuration of the tracked signals. This demonstrates that current technology can achieve highly coherent clock tracking in a lab environment.

# 5    Conclusions

The proof-of-concept of the GNSS-based phase synchronization conducted in this study was successful. The precision achieved by the technique depends on several factors. The main performance drivers identified in the experiment were the reference tracking precision of the receiver and multipath suppression. Through the experiments, we discovered that the accuracy of the technique can be increased considerably through appropriate inspection of the signals, calibration of the covariance matrix of the measurement, and appropriate optimized filtering.

The results show that the GNSS-based synchronization ha the potential to be a simple and scalable solution for bistatic and multistatic systems, which could guarantee compatibility of different systems designed and launched completely independently, opening many possibilities for data combinations across missions operating in the same band. They show that current technology could potentially achieve sufficient accuracy up to the C-band and hint at the potential of applicability to systems up to the X-band with incremental changes to currently available technology or the use of better-performing devices, as long as the previously identified main error contributions, such as multipath and cross-talk, are either suppressed or mitigated.

# 6    Acknowledgements

# 7    Literature

[1]   N. Ustalli, G. Krieger, J. Mittermayer, M. Villano, and C. Waldschmidt: MirrorSAR Concept: Phase Synchronization Analysis, Kleinheubacher Tagung, Miltenberg, Germany, 2022

[2]   E. Rodrigues-Silva and M. Rodriguez-Cassola: Analysis of a POD-based Approach for Phase and Time Synchronization of Bistatic and Multistatic SAR Systems, EUSAR 2021; 13th European Conference on Synthetic Aperture Radar, online, 2021

[3]   M. N. Peixoto, G. Krieger, A. Moreira, C. Waldschmidt and M. Villano: On the Exploitation of CubeSats for Highly Accurate and Robust Single-Pass SAR Interferometry, in IEEE Transactions on Geoscience and Remote Sensing, 2023

[4]   N. Sakar, M. Rodriguez-Cassola, P. Prats-Iraola and A. Moreira: Azimuth Reconstruction Algorithm for Multistatic SAR Formations With Large Along-Track Baselines, in IEEE Transactions on Geoscience and Remote Sensing, vol. 58, no. 3, pp. 1931-1940, March 2020

[5]   U. Weinbach, S. Schon and T. Feldmann: Evaluation of state-of-the-art geodetic GPS receivers for frequency comparisons, 2009 IEEE International Frequency Control Symposium Joint with the 22nd European Frequency and Time forum, Besancon, France, pp. 263-268, 2009

[6]   G. Krieger, H. Fiedler, I. Hajnsek, M. Eineder, M. Werner, A. Moreira: TanDEM-X: mission concept and performance analysis. In International Geoscience and Remote Sensing Symposium, vol. 7, p.4890. 2005.

[7]   G. Jin et al.: An Advanced Phase Synchronization Scheme for LT-1, in IEEE Transactions on Geoscience and Remote Sensing, vol. 58, no. 3, pp. 1735-1746, March 2020

[8]   M. Grasso, A. Renga, G. Fasano, M.D. Graziano, M. Grassi, and A. Moccia: Design of an end-to-end demonstration mission of a formation-flying synthetic aperture radar (FF-SAR) based on microsatellites, Advances in Space Research, vol. 67, no. 11, pp. 3909–3923, 2021

[9]   Krieger, G., Zink, M., Bachmann, M., Bräutigam, B., Schulze, D., Martone, M., Rizzoli, P., Steinbrecher, U., Antony, J.W., De Zan, F. and Hajnsek, I., Papathanassiou, K., Kugler, F., Rodriguez-Cassola, M., Younis, M., Baumgartner, S. López-Dekker, F., Prats, P. and Moreira, A: TanDEM-X: A radar interferometer with two formation-flying satellites. Acta Astronautica, 89, pp.83-98, 2013.

[10]   Lombardi, M. A., Nelson, L. M., Novick, A. N., Zhang, V. S.: Time and frequency measurements using the global positioning system. Cal Lab: International Journal of Metrology, 8(3), 26-33, 2001.

[11]   Sandenbergh, Jacobus S: Synchronising coherent networked radar using low-cost GPS-disciplined oscillators. PhD Thesis, University of Cape Town, 2019.

[12]   W.-Q. Wang: Gps-based time phase synchronization processing for distributed sar. IEEE Transactions on Aerospace and Electronic Systems, vol. 45, no. 3, pp. 1040–1051, 2009.